

Electronic charge density modulations in the disordered film of titanium nitride

P. Kulkarni*, H. Suderow, J.Rodrigo, and S. Vieira

*Laboratorio de Bajas Temperaturas, Departamento de Física de la Materia Condensada,
Instituto de Ciencia de Materiales Nicolás Cabrera, Facultad de Ciencias,
Universidad Autónoma de Madrid, 28049 Madrid, Spain*

M.R. Baklanov

IMEC, Kapeldreef 75, B-3001 Leuven, Belgium

T. Baturina

Institute of Semiconductor Physics, 13 Lavrentjev Avenue, Novosibirsk, 630090, Russia

V. Vinokur

Materials Science Division, Argonne National Laboratory, Argonne, Illinois 60439, USA

(Dated: December 3, 2024)

We report in this paper the atomic level imaging in the polycrystalline film of titanium nitride. The crystalline boundaries are resolved at several places on the film surface, and the atomic positions are clearly seen with different orientations. We also observed presence of electronic charge density modulations, with their wave vectors varying over a large range, and in several directions. We associate the presence of charge density modulations to the disorder scattering of electronic waves at the low angle crystalline boundaries. We further consider the effect of Charge density modulations on the superconducting phase. In the STS measurement, we find that the conductance fluctuations at energies close to the superconducting gap are strongly influenced by the charge modulation patterns. At quasi-particle peak position and near zero bias, the conductance fluctuations are relatively suppressed.

PACS numbers: 74.55.+v, 74.78.-w, 74.62.En, 74.81.-g

Superconductor to insulator transition can be induced with disorder, or the magnetic field in thin superconducting films[1–10]. Several disordered superconducting films were studied to understand the microscopic drive of the superconductor to insulator transition. Popular approaches in theoretical and transport measurements being to perceive the changes in the superconducting order parameter, or the disorder enhanced Coulomb interactions close to SIT. The local tunneling measurements to a large extent supported the fluctuations of the superconducting order parameter. However, these measurements till now were not based on the high resolution simultaneous topographic information. As the films are made more disordered, the likelihood of Coulomb interactions enhances, and the subsequent changes on the continuous superconducting phase are highly probable.

Many interesting local tunneling experiments addressed the effect of disorder on the superconducting phase. Intrinsic inhomogeneities were reported as a function of amplitude fluctuations in strongly disordered TiN films[11] or phase fluctuations in NbN films[12]. In homogeneously disordered InO films, STS measurements of the tunneling spectra were reported close to SIT. It was shown that the quasi-particle peaks tend to suppress with increase in disorder while the superconducting gap remains intact[13]. Direct localization of the preformed cooper pairs was suggested as the precursor to the SIT. On the other hand the evolution of the tunneling spectra

with temperature in TiN films suggested the pseudo-gap like behavior[14], which was considered as a precursor to the superconducting phase. Pseudo-gap features were also shown to enhance with the increase in the disorder. These studies were aimed at observing the local changes in the superconducting phase at different levels of disorder. However, the role of Coulomb interactions remained obscure in local measurements. We chose well characterized TiN films[9, 10, 15] to study the atomic level topographic and high resolution spectroscopic images using STM/S at 100 mK. Our measurements reveal possibilities to observe the role of Coulomb interactions and superconductivity in the disordered films.

The titanium nitride film is deposited using Atomic layer chemical vapour deposition technique at 350 degree on Si/SiO₂ substrate. The film thickness was 5 nm and the microstructure consists of densely packed crystallites with low angle boundaries. The crystallite size range was estimated as 3 to 10 nm, with average size around 5 nm. TiN has FCC structure with the atomic distance between (100) planes as 4.2 Å. In Figure 1, the positions of Ti and N ions are shown in the unit cell. A STM image of the film is also shown in Figure 1, where several crystallites are visible and the histogram in the inset shows their size distribution.

Figure 2 shows the atomic level image measured over an area 10 nm x 10 nm. The atomic positions are visible and form regular arrays in two directions. The height

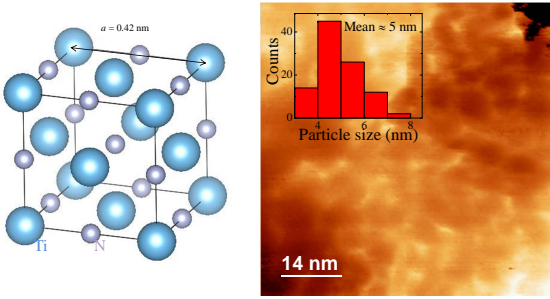


FIG. 1: The crystal structure of titanium nitride with Ti atoms forming the FCC unit cell, and the N atoms occupying the positions at the centre, and on the edges. The lattice parameter for [100] plane is shown as 0.42 nm. The main panel in the right shows the STM surface image for the TiN film. The crystallite sizes were estimated and presented in the form of the histogram shown in the inset.

variations in the image are less than 0.5 nm. A 2d-FFT of the atomic level image is shown in panel (b), where it is easier to locate the periodic structures. A simple $1/\text{wavelength}$ formula is used to make the 2d-FFT images presented in this paper. In panel (b), several bright spots are seen, regularly arranged forming replicas of two dimensional atomic lattice seen in panel (a). The distances of the first set of bright spots from the centre are measured and converted in the units of lattice parameter a for TiN. As highlighted in the panel (b), these would correspond to [200] and [110] sets of atomic planes in FCC structure of TiN.

In figure 3(a), we show an image over 12.4 nm x 12.4 nm. At this position, two sets of atomic planes are seen, corresponding to different crystallites separated by a sharp boundary. The black lines show the directions of the atomic planes. We choose the crystallite in the lower part in the panel (a), and make its 2d-FFT image, as shown in panel (b). Four bright spots are encircled using black lines. The distances adjusted in the units of the lattice parameter suggest that the planes correspond to [111] and [210]. When we use the bright spots to filter out the other intensities in the FFT image, the atomic lattice is obtained as shown in the inset in panel (b).

Figure 4 (a) to (d) shows the topographic images with four different scan sizes. The corresponding 2d-FFT images are shown in panels (e) to (h). In panel (a) over a large scale image with an area about 512 nm x 512 nm, several bright lines are observed. With small area scans, 56.9 nm x 56.9 nm in panel (b) and 42.7 nm x 42.7 nm in panel (c), these lines are resolved as charge

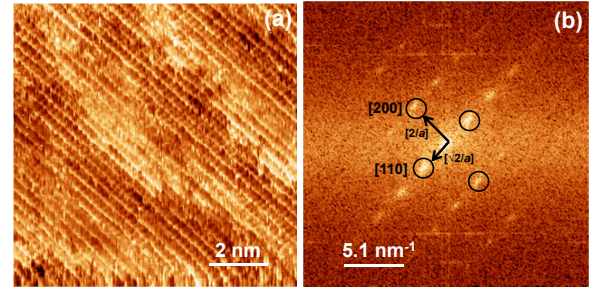


FIG. 2: In panel (a) Atomic level image over an area 10 nm x 10 nm in TiN film is shown. The 2d-FFT image is shown in panel (b). The first set of four bright spots are encircled using black color line. Arrows show the distances in the units of lattice parameter a and the corresponding the planes are labeled in the square brackets.

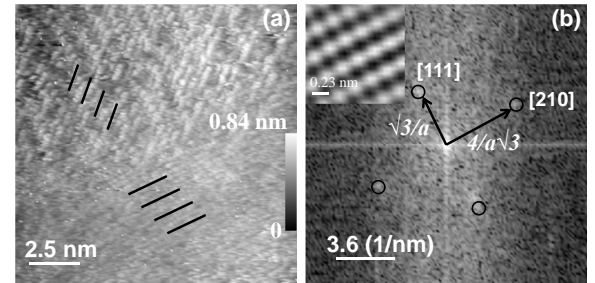


FIG. 3: In panel (a) the image over 12.4 nm x 12.4 nm shows two atomic orientations, schematically shown by the set of black lines. The height scale is shown on the right of the panel to estimate the changes in the topographic features. In panel (b) the 2d-FFT image is shown for the crystallite on the bottom in panel (a). The four bright spots are encircled using black lines and their distances are estimated in units of a . The inset in panel (b) shows the filtered atomic lattice using the four bright spots.

density modulations coherent over large distances and overlapping considerably forming beat patterns. The intensity at these overlapped regions becomes stronger, and in the larger area scans, the beats are seen as lines. In the panel (e), the FFT image shows intensities mainly in two orientations, falling off exponentially as shown by the

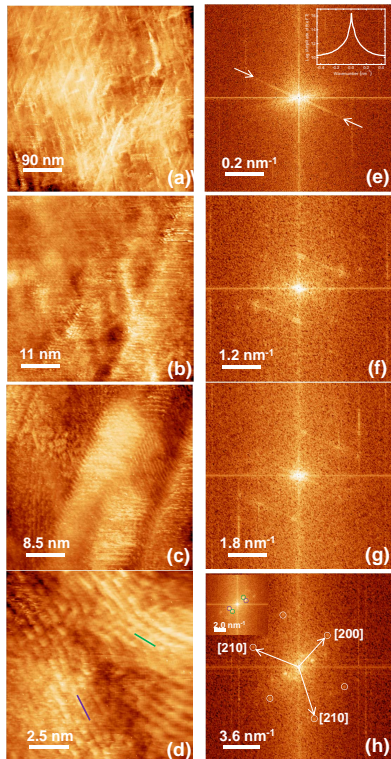


FIG. 4: Panels (a) to (d) show the topographic images over large to smaller areas. In panels (e) to (h) are corresponding 2d-FFT images.

line profile in the inset. In the 2d-FFT images in panels (f) and (g), for smaller scan areas, the bright spots are seen forming rectangular positions, corresponding to the charge density modulations.

In panel (d) in Figure 4, the image is shown over $12.7 \text{ nm} \times 12.7 \text{ nm}$. Two orientations of the charge modulations can be seen along with the atomic level features in the topographic image. A blue and green color lines identify these two orientations. In panel (h), we show the 2d-FFT image of panel (d) along with the magnified portion in the inset. We observe four bright spots, for two orientations of the charge modulations, encircled with green and blue lines, respectively. At smaller wavelengths, as shown in the main panel (h), six bright spots are circled using black lines, marking the underlying hexagonal atomic positions in the image in panel (d). The distances of these bright spots in the units of lattice parameter a would form the planes $[210]$ and $[200]$.

In Figure 5 (a), we show topographic image over $16.6 \text{ nm} \times 16.6 \text{ nm}$. The numerals in the image, 1 to 3, are representatives of three regions. 1 and 3 correspond to the two crystallites, which are seen with different atomic orientations. The boundary between these two regions is marked by numeral 2, where formation of charge den-

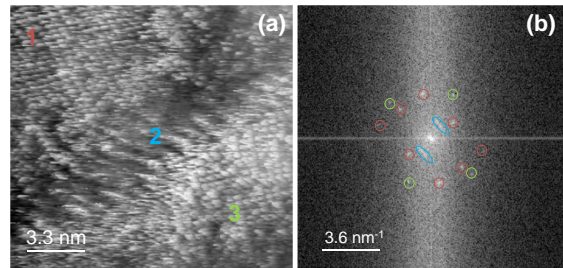


FIG. 5: In panel (a) a $16.6 \text{ nm} \times 16.6 \text{ nm}$ topographic image is shown, which display orientations of the two crystallites represented by numerals 1 and 3. The crystalline boundary is represented by the numeral 2. Panel (b) shows the 2-FFT image with the bright spots corresponding to the three different regions.

sity modulations can be seen. In the panel (b), the 2d-FFT image of panel (a), three configurations of the bright spots are seen. The encircled green spots represent the atomic orientations in the crystallite, marked by 3, in panel (a). The encircled red spots are FFT of the crystallite, marked by 1. A change of atomic orientations from 3 to 1 is about 30 degrees. The light blue spots with longer wavelengths represent the periodicity of the charge density modulations, which are seen confined at the crystalline boundary. This highlights the role of crystalline boundaries in disorder electron scattering and possibly the formation of standing wave patterns on the film surface. Such electron scattering at the crystalline boundaries may also result in the enhanced electron-electron repulsion effect [16–18], in the 2-d disordered films.

In figure 6, we show the STS measurement over an area $512 \text{ nm} \times 512 \text{ nm}$. This is the same region which is shown in panel (a) in Figure 4. At all the positions, the superconducting gap opens. The representative tunneling spectra is shown in the inset in panel (a). The positions of the quasi-particle peaks is around 0.5 mV and the rough estimation of the superconducting gap is close to 0.25 mV . We measured 128×128 tunneling curves in an area $512 \text{ nm} \times 512 \text{ nm}$. The STS maps were made between -1 mV to $+1 \text{ mV}$ after the tunneling curves were normalized at 1 mV . In panel (a) to (c), the conductance maps are shown at three selected bias voltages, $V = 0.0, 0.25$ and 0.5 mV . The maps are visuals of the spatial conductance distribution at the bias voltage mentioned at the bottom right corner in each panel. In panels (d) to (f), the 2d-FFT images of the respective conductance maps are shown. At zero bias voltage, the conductance

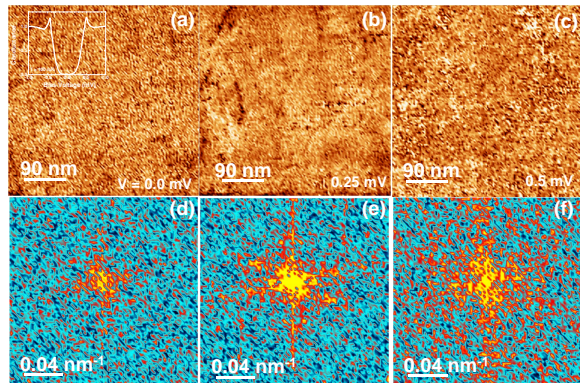


FIG. 6: Panels (a) to (c) are the conductance maps at the selected bias voltages, 0.0, 0.25 and 0.5 mV. Inset in panel (a) shows the representative superconducting density of states normalized at 1 mV. The panels (d) to (f) show the 2d-FFT images of the conductance maps in panels (a) to (c), respectively.

map shows relatively uniform distribution, as also seen in the 2d-FFT image in panel (d). At 0.25 mV, the conductance distribution produces beating patterns, those also seen in the topographic images in panel (a) of Figure 4. This value of bias voltage is very close to the superconducting energy gap in this film. In the 2d-FFT image in panel (e), we observe intensities extending in two directions, showing clearly the changes in the conductance distribution following the beat patterns similar to those in panel (e) in Figure 4. At the position of quasi-particle peaks, these changes are smeared out. This is shown in panel (f) in the figure. Our measurements suggest that the effect of the disorder electron scattering on the superconducting phase is to produce concurrent conductance fluctuations at energies close to the superconducting energy gap at the beat positions.

In conclusion, we observed atomic level images on the amorphous substrate using STM imaging at 100 mK. Crystalline boundaries are resolved, and their role in forming the charge density modulations was highlighted. Beat patterns due to electronic wave interference were analyzed to study the effect on the superconducting phase.

We acknowledge support of UAM workshop SEGAIN-

VEX. This work was supported by the Spanish MINECO (Consolider Ingenio Molecular Nanoscience CSD2007-00010 program, FIS2011-23488 and Indo-Spain collaboration ACI-2009-0905), by the Comunidad de Madrid through program Nanobiomag-net (S2009/MAT-1726), by the program Quantum mesoscopic and disordered structures of the Russian Academy of Sciences, by the Russian Foundation for Basic Research (Grant No. 12-02-00152 and Grant No. 12-02-31302), and by the US Department of Energy Office of Science under the Contract No. DEAC02-06CH11357.

-
- [1] M. Strongin, R. S. Thompson, O.F. Kammerer, and J. E. Crow, *Phys. Rev. B* 1, 1078 (1970).
 - [2] D. B. Haviland et al., *Phys. Rev. Lett.* 62, 2180 (1989); Y. Liu et al., *Phys. Rev. B* 47, 5931 (1993).
 - [3] S. Okuma, T. Terashima, and Kokubo, *Phys. Rev. B* 58, 2816 (1998).
 - [4] V. F. Gantmakher et al. *JETP* 82, 951 (1996).
 - [5] Y. Qin, C. L. Vicente, J. Yoon, *Phys. Rev. B* 73, 100505(R) (2006)
 - [6] E. Bielejec, J. Ruan, and W. Wu, *Phys. Rev. Lett.* 87, 36801 (2001).
 - [7] M. P. A. Fisher, and D. H. Lee, *Phys. Rev. B* 39, 2756 (1989).
 - [8] A. F. Hebard, and M. A. Paalanen, *Phys. Rev. Lett.* 65, 927 (1990).
 - [9] T. I. Baturina et al. *Phys. Rev. Lett.* 99, 257003 (2007).
 - [10] T. I. Baturina et al., *Pisma v ZhETF* 79, 416 (2004) [*JETP Lett.* 79, 337 (2004)].
 - [11] B. Sacepe, C. Chapelier, T. I. Baturina, V. M. Vinokur, M. R. Baklanov, and M. Sanquer, *Phys. Rev. Lett.* 101, 157006 (2008).
 - [12] Y. Noat, T. Cren, C. Brun, F. Debontridder, V. Cherkez, K. Ilin, M. Siegel, A. Semenov, H. Hubers, and D. Roditchev *ArXiv* 1205.3408 (2012).
 - [13] B. Sacepe et al., *Nature Physics* 7, 239 (2011).
 - [14] B. Sacepe, C. Chapelier, T. I. Baturina, V. M. Vinokur, M. R. Baklanov, and M. Sanquer, *Nature Communications* 1, 140 (2010).
 - [15] F. Pfuner, L. Degiorgi, T. I. Baturina, V.M. Vinokur, M. R. Baklanov, *New J. Phys.* 11, 113017 (2009).
 - [16] B. Altshuler, A. Aronov, and P. Lee, *Phys. Rev. Lett.* 44, 1288 (1980).
 - [17] B. Altshuler, and A. Aronov, Elsevier, *Electron Electron Interaction in Disordered Conductors* (1985).
 - [18] L. Bartosch, and P. Kopietz, *Eur. Phys. J.* 28, 29 (2002).